Analyst

ROYAL SOCIETY OF CHEMISTRY

PAPER

View Article Online
View Journal | View Issue

Cite this: *Analyst*, 2020, **145**, 4352

An enhanced gas sensor based on SiO_2@mesoporous MCM-41 core–shell nanocomposites for SO_2 visual detection†

Ji Yang,[a] Fuqiang Cheng,[a] Zuogang Zhu,[b] Jinsheng Feng,[a] Min Xue,[a] Zihui Meng *[a] and Lili Qiu [a]

Received 30th March 2020,
Accepted 14th May 2020

DOI: 10.1039/d0an00621a

rsc.li/analyst

A colorimetric sulfur dioxide (SO_2) gas sensor based on a core–shell composite was developed. The composite was fabricated with a silicon dioxide core and a mesoporous MCM-41 shell (SiO_2@MCM-41), and further loaded with a mixture of zinc chloride ($ZnCl_2$), sodium nitroprusside (SNP) and hexamine as an SO_2 indicator. The sensing properties of SiO_2@MCM-41 toward SO_2 were measured in solid powder, discs and a gas detection tube (GDT), respectively. Each of these sensing configurations showed a distinct color change from pale yellow to red, which indicates good potential for naked-eye detection of SO_2. The limit of detection (LOD) is 2 ppm for SiO_2@MCM-41 discs, which indicates high sensitivity to SO_2. The performance of GDT suggested a linear relationship between the SO_2 concentration and the response length of the red portions in a range of 100–1000 ppm. This work shows promising potential of SiO_2@MCM-41 as an easy, effective and rapid response sensing material for the *in situ* detection of SO_2.

Introduction

SO_2 has drawn worldwide attention as one of the major pollutants in the atmosphere, and is mainly produced from the burning of fossil fuels. After dissolving in water vapor, SO_2 can interact with other particles in air and form an acid.[1–4] The emission of SO_2 has contributed to a series of problems that threaten the environment and human health, such as acid rain, eye irritation, and respiratory illnesses. The acid rain has caused great losses in forestry, agriculture, aquaculture, animal husbandry, and construction.[5–7] Moreover, the acid rain areas of China are the world's third largest acid rain areas next to Europe and North America, which have reached 30% of the total land area.[8] Without effective monitoring, air pollution and environmental acidification caused by the acid rain will increase. Therefore, it is significant to develop an SO_2 sensor with quick and accurate detection. Various approaches, including optics, semiconductor and electrolyte technologies, have been used to detect SO_2.[9–12] However, the abovementioned methods for SO_2 detection usually suffer from the requirement of expensive instruments and complicated operation and are inconvenient for on-site monitoring.[13,14]

In the early 1990s, scientists in Mobil prepared M41S silicate mesoporous molecular sieves with highly uniform and ordered pore structures, which extend the pore size from micropores to mesopores.[15] Mesoporous materials have been vastly studied as adsorbents, sensors, catalysts, and drug carriers because of their high specific surface areas, tunable pore sizes, high mechanical strength and capability of chemical functionalization.[16–20] Various mesoporous materials have been reported for sensing. For example, mesoporous semiconductor metal oxides are widely used for gas sensing. Zhao *et al.* synthesised ordered mesoporous Fe doped In_2O_3 for NO_2 gas sensing, and the as-prepared sensor exhibited an excellent response to NO_2 gas.[21] Izu *et al.* fabricated a $V_2O_5/WO_3/TiO_2$ resistive sensor for SO_2 detection, and the response range is from 20 to 5000 ppm.[22]

Although mesoporous materials have great potential in different areas, it is gradually becoming difficult for single-component mesoporous materials to meet the requirements of various applications. Recently, multifunctional mesoporous composites with a controlled microstructure, which can overcome the deficiencies of single-component mesoporous materials, have attracted increasing attention. Core–shell composites are nanostructures that have a core that is coated by another material, and they have been extensively explored for their unique structures and properties.[23] The hybrid structures of core–shell nanoparticles enhance the chemical and thermal stability. Also, the combined functionalities of cores and shells can allow them to achieve synergistic functions and have good

[a]*School of Chemistry & Chemical Engineering, Beijing Institute of Technology, Beijing 100081, PR China. E-mail: m_zihui@yahoo.com*
[b]*Beijing Municipal Institute of Labor Protection, Beijing 100054, PR China*
†Electronic supplementary information (ESI) available. See DOI: 10.1039/d0an00621a

potential for applications in various research fields.[24–27] In particular, considering the high surface to volume ratio, core–shell mesoporous materials can enhance the gas sensing performance. Wu *et al.*[28] fabricated hematite hollow spheres with a mesoporous shell, and the obtained α-Fe_2O_3 exhibited high gas sensitivity toward formaldehyde and ethanol at room temperature. Li *et al.*[29] proposed an NH_3 sensor based on a Au-loaded mesoporous In_2O_3 nanosphere@polyaniline core–shell nanohybrid, and the sensor showed excellent sensitivity, selectivity and reproducibility to NH_3 at room temperature.

Gas sensing involves the adsorption and desorption processes on the surfaces of materials, and core–shell mesoporous materials with high surface specific areas are favorable for gas diffusion. Herein, we report core–shell silica nanoparticles with a silica core and ordered mesoporous silica shell for SO_2 sensing. The SiO_2 core was synthesized based on the Stöber method,[30] and the mesoporous MCM-41 shell was obtained by using cetyltrimethyl ammonium bromide (CTAB) as a template. $ZnCl_2$, SNP and hexamine were mixed as an SO_2 indicator, which was loaded on the surface of MCM-41. The sensing performance of SO_2 gas was measured by the as-prepared SiO_2@MCM-41 in 3 different forms, and each form of SiO_2@MCM-41 involved a distinct color change. Additionally, the SiO_2@MCM-41 sensor exhibited remarkable repeatability, high sensitivity and perfect response concentration linearity to SO_2 at room temperature, which suggests its promising applications for SO_2 gas sensing.

Experimental

Chemicals & apparatus

Glycerin, SNP, $ZnCl_2$, hydrochloric acid and hexamine were purchased from Beijing Chemical Plant. Sodium hydroxide (NaOH) and anhydrous sodium sulfate were obtained from Beijing Tongguang Fine Chemicals Co. Ltd. Tetraethyl orthosilicate (TEOS), CTAB, ethanol, isopropanol, and ammonium hydroxide ($NH_3{\cdot}H_2O$) were purchased from J&K Scientific Ltd.

The heating process was carried out in a DNP-9022 electrothermal incubator (Jinghong). The calcination of SiO_2@MCM-41 was carried out in a muffle furnace (Yiheng, SX2-8-10NP). The microstructure was characterized using a scanning electron microscope (SEM) (Hitachi, S-4800) and a transmission electron microscope (TEM) (JEM-2100, JEOL). The porous properties of SiO_2@MCM-41 were investigated by nitrogen adsorption and desorption at 77.3 K using an ASAP 2020, Micromeritics Instrument Corp, USA. The pore-size-distribution curves were obtained from the adsorption branches using non-local density functional theory (NLDFT).

Synthesis of SiO_2@MCM-41 composites

Preparation of SiO_2@MCM-41 core–shell nanoparticles. SiO_2 nanoparticles were prepared according to a previously published method.[31] Briefly, 2 mL TEOS was added to 2 mL $NH_3{\cdot}H_2O$, 20 mL deionized H_2O and 200 mL isopropanol at 35 °C under magnetic stirring. After stirring for 2 h, the resultant mixture was collected by centrifugation, followed by washing with ethanol and water 3 times. The above obtained SiO_2 nanospheres were dispersed in the mixed solution of 100 mL ethanol and 200 mL deionized H_2O. 2 mL of 1 mol L^{-1} NaOH was added into the above solution under 500 rpm magnetic stirring for 30 min. Then, 2 g CTAB was added to the mixture. After 30-minute-stirring, 0.45 mL TEOS was added to the mixture. The product was collected by centrifugation after reaction for 8 h and then washed repeatedly with ethanol and water to remove the template CTAB. Finally, the as-prepared products were heated in a muffle furnace to 550 °C for 6 h and SiO_2@MCM-41 nanoparticles were produced.

Preparation and loading of the SiO_2@MCM-41 indicator. The SiO_2@MCM-41 indicator was prepared by dissolving 1 g $ZnCl_2$ in 10 mL ultrapure water with 0.5 mL hydrochloric acid, 1 g SNP in 10 mL ultrapure water with 0.5 mL glycerol, and 2 g hexamine in 10 mL ultrapure water. Afterward, we added 0.1, 0.2 and 0.1 mL as-prepared $ZnCl_2$, SNP and hexamine solution to 30 mg SiO_2@MCM-41 solid powder, respectively. After mixing the solution with SiO_2@MCM-41 uniformly, the powder was dried in an oven for 30 min at 80 °C. The mechanism of $ZnCl_2$, SNP and hexamine as an SO_2 indicator was referred to a previous report.[32] Before SiO_2@MCM-41 was loaded with the SO_2 indicator, we weighed the SiO_2@MCM-41 solid powder with an electric balance, and the weight was found to be 563 mg. Then we treated SiO_2@MCM-41 with the SO_2 gas indicator and dried it in an oven. After the powder was completely dried, we weighed it again, and the weight was 576 mg. The weight of the SiO_2@MCM-41 solid powder increased after being loaded with the SO_2 indicator; so we suggested that the indicator was loaded successfully.

Gas sensing measurement

SiO_2@MCM-41 solid gas sensing test. The gas sensing test was carried out on an as-fabricated gas sensing system, which is shown in S1.† SiO_2@MCM-41 solid samples were placed inside an airbag (1L) and then different ratios of SO_2 and air were injected. After the balance between SO_2 adsorption and desorption, the color change of the SiO_2@MCM-41 solid samples was recorded.

Gas adsorption test. The concentration of sulfate ions in solution can be obtained by ion chromatography.[33] 1.479 g anhydrous sodium sulfate was dissolved in ultrapure water and transferred to a 1 L volumetric flask as a sulfate ion stock liquid. We added 0.5, 1, 2.5, 5 and 7.5 mL of the sulfate ion stock liquid to 10 mL volumetric flasks, respectively. Sequentially, 50, 100, 250, 500 and 750 mg L^{-1} sulfate ion standard solutions were obtained. Then, 30 μL of each concentration sulfate ion standard solution was injected into the ion chromatography system, and a standard working curve was prepared based on the chromatographic peak area (S2).†

For the measurement of the gas adsorption rate of the SiO_2@MCM-41 solid samples, first, 100 mL of 0.2 mol mL^{-1} NaOH solution and hydrogen peroxide solution were mixed as the SO_2 adsorption solution. Afterward, we placed 30 mg of the SiO_2@MCM-41 solid samples inside an airbag and injected

50 ml of SO_2 at 15 °C. While waiting for the balance of gas adsorption, the remaining gas in the airbag was delivered into a sealed container with the as-prepared SO_2 adsorption solution. After adsorption at 5 °C for 6 h, sulfate ions were detected by ion chromatography. Then the concentration of sulfate ions in the as-prepared SO_2 adsorption solution can be obtained from the standard working curve. According to the amount of sulfate ions, the adsorption rate of SO_2 was calculated.

3SO_2 gas detection tube (GDT) test. A homemade sensing system of SO_2 GDT is presented in S3.† We injected different concentrations of SO_2 gas prepared in airbags through a tube using a 100 mL syringe. After the gas passed through the SO_2 GDT, it was collected by another 100 mL syringe, which was connected to the end of the tube. For each concentration, the experiment was repeated 10 times, and the color change and response length of the SO_2 GDT were recorded. Scheme 1 shows a schematic illustration of the fabrication and sensing processes of SiO_2@MCM-41.

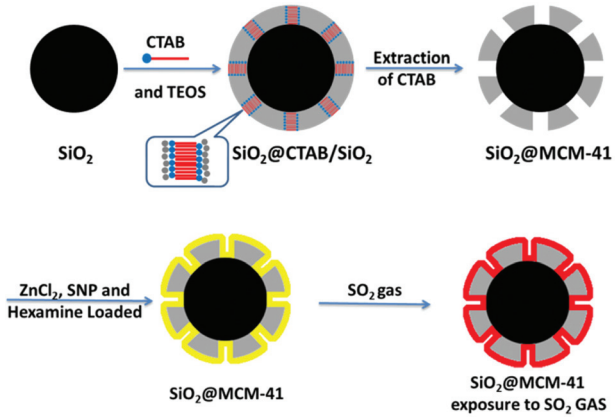

Scheme 1 Schematic illustration of the fabrication and detection processes of SiO_2@MCM-41.

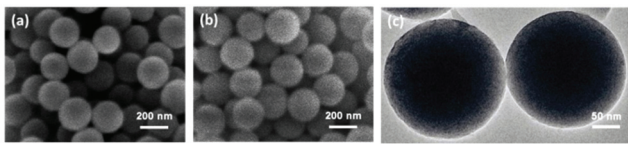

Fig. 1 SEM images of (a) SiO_2 nanoparticles and (b) SiO_2@MCM-41 composite nanoparticles. (c) TEM image of SiO_2@MCM-41 composite nanoparticles.

Results and discussion

Characterization of SiO_2@MCM-41

From the SEM image (Fig. 1a), the mean diameter of SiO_2 particles is found to be 206 ± 5 nm, and the sizes of these particles are uniform. SiO_2 nanoparticles showed good monodispersity and sphericity. After the combination of SiO_2 with MCM-41, the SEM image showed that the mean diameter of SiO_2@MCM-41 increased to 235 ± 5 nm, and the TEM image revealed a distinct core–shell structure of SiO_2@MCM-41 composite nanoparticles, and both implied that the MCM-41shell integrated with the SiO_2 core successfully (Fig. 1b and c). The adsorption curves of SiO_2@MCM-41 exhibited the type-IV isotherm (Fig. S4†), which is characteristic of mesoporous materials. A Brunauer–Emmett–Teller (BET) surface area of 656 $m^2\ g^{-1}$ was estimated for SiO_2@MCM-41. The NLDFT gave rise to a narrow pore size distribution with an average pore width of 10.6 nm (Fig. S4†).

The visual detection of SO_2

The response of the SiO_2@MCM-41 nanocomposite toward SO_2 was investigated over a range of 100–8000 ppm, and the results are presented in Fig. 2. After exposure to SO_2, the color of the SiO_2@MCM-41 nanocomposite changed from pale yellow to red visually. In the presence of SO_2 with different concentrations, the powder showed a different color. In this enclosed environment of SO_2, the observed response time is typically around 20 s. Based on the above experiment studies and literature findings, we proposed a mechanism for the sensing of SiO_2@MCM-41. After the gas adsorption, SO_3^{2-} is generated. When SNP and SO_3^{2-} are mixed, a deep red coloration develops. The coloration results from what is commonly

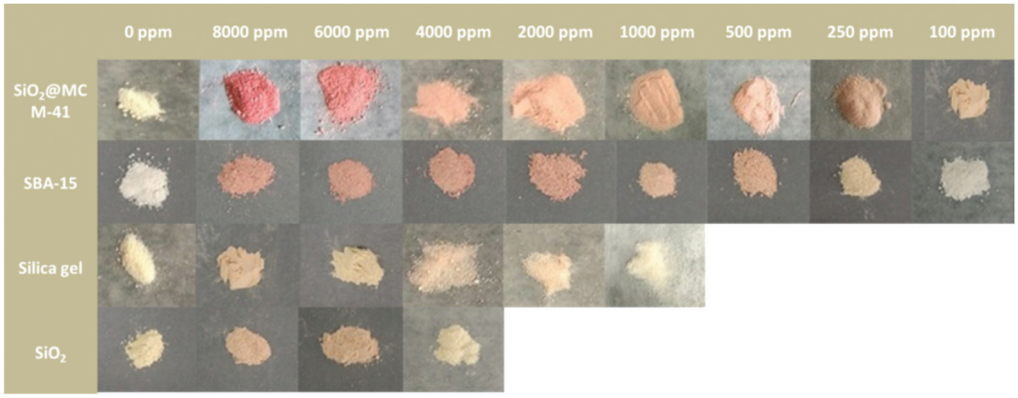

Fig. 2 The visual color changes of SiO_2@MCM-41, SBA-15, silica gel and SiO_2 in response to different concentrations of SO_2 gas.

called the Boedeker reaction.[34] SNP and sulfite interact to give the red, highly dissociated sulphitonitroprusside ions as follows:

$$Fe(CN)_5\ NO^{2-} + SO_2{}^{-3} \rightleftharpoons Fe(CN)_5\ NOSO_3{}^{4-}$$

According to the previous research,[35] the addition of zinc ions results in the formation of sparingly soluble zinc sulphitonitroprusside and markedly increases the sensitivity of the Boedeker reaction. The alkaline medium can form ion-pairs of the type $Fe(CN)_5\ NOSO_3M^{3-}$, where M is an alkaline medium. So we added $ZnCl_2$ and hexamine to help increase the sensitivity of the Boedeker reaction. Also, the larger the volume of SO_2 that SiO_2@MCM-41 adsorbed, the larger the volume of sulphitonitroprusside ions it reacted with, so that the color change of the response becomes more significant.

The SO_2 sensing properties for other porous solids were also measured (Fig. 2). The SiO_2@MCM-41 nanocomposite exhibits a higher response than SBA-15, silica gel and SiO_2, which is in agreement with their adsorption properties. Compared to SiO_2@MCM-41, the color changes of these materials are less obvious. The LOD value of SiO_2@MCM-41 is lower than 100 ppm while the LOD values of SBA-15, silica gel and SiO_2 are 250 ppm, 2000 ppm and 6000 ppm, respectively. These results are due to the difference in the specific surface areas of these solids. SiO_2@MCM-41 has a higher specific surface area than others, which can provide more binding sites and lead to more rapid adsorption of SO_2 on the surface.

The adsorption properties of the SiO_2@MCM-41 solid

The reproducibility of the SiO_2@MCM-41 sensing system was evaluated as the weight changes of SiO_2@MCM-41 for 10 cycles (Fig. 3a). The SiO_2@MCM-41 nanoparticles were alternately placed under air and SO_2 atmosphere at 15 °C. The initial weight of the solids was 540 mg in air, and changed to ~691 mg after exposure to SO_2 gas. With the adsorption and desorption of SO_2 from the pore structure of SiO_2@MCM-41, the weight changed and the adsorption rate was maintained after 10 cycles. Moreover, after SO_2 gas bound with the indicator that loaded on SiO_2@MCM-41, the nanoparticles changed from white to red accordingly. The color change of SiO_2@MCM-41 upon exposure to SO_2 and air is reversible, which implies the remarkable stability and repeatability of this sensor.

Fig. 3b illustrates the adsorption capacity of a series of nanoparticles including SiO_2@MCM-41, SBA-15, silica gel and SiO_2. Owing to the porous structure and high specific surface area of SiO_2@MCM-41, which allow them to adsorb more gas, the adsorption capacity of SiO_2@MCM-41 is higher than that of other porous materials. The adsorption rate for SO_2 is 28% for SiO_2@MCM-41 while the rates are 23%, 10% and 4% for

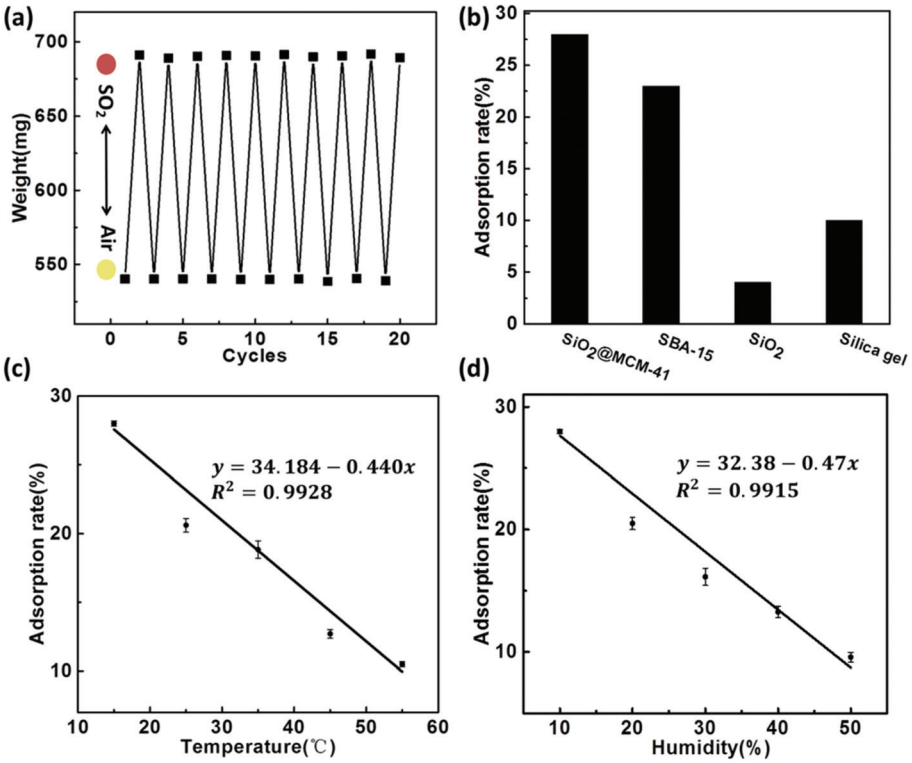

Fig. 3 (a) Reversible changes of the weight of SiO_2@MCM-41 when alternately exposed to air and SO_2 gas, and the corresponding color changes. (b) The adsorption rates of SiO_2@MCM-41, SBA-15, silica gel and SiO_2 toward SO_2 gas. (c) The relationship between the adsorption rate and the temperature of SO_2 gas. (d) The relationship between the adsorption rate and the humidity of SO_2 gas.

SBA-15, silica gel and SiO_2. Hence, we believe that SiO_2@MCM-41 is an ideal material for SO_2 gas sensing.

For practical applications, temperature and humidity are critical influencing factors for gas sensors. Fig. 3c and d show how the adsorption rate toward SO_2 varies with its temperature and humidity, respectively. With the increasing temperature, the absorption capacity decreased, suggesting an exothermic process (Fig. 3c). This indicated that low temperature is in favor of SO_2 absorption. In a high-moisture environment, water vapor can block the adsorption sites on the surface of SiO_2@MCM-41 and compete with SO_2 gas for these sites. As a result, the adsorption rate for SO_2 decreased (Fig. 3d). These adsorption behaviours under different temperatures and humidity are consistent with the references.[36–38]

SO_2 sensing properties

The SiO_2@MCM-41 solid was pressed into discs with a manual hydraulic press at 20 MPa to detect the gases of low-concentration SO_2 (Fig. 4). When the SO_2 gases with different concentrations were injected into the airbag, these discs exhibited different color changes in 10 s. With the increase of the SO_2 concentration, more red reaction products were obtained and the color change became more obvious. Moreover, the LOD of SiO_2@MCM-41 was also investigated. When the concentration of SO_2 is lower than 2 ppm, the amount of gas SiO_2@MCM-41 absorbed is too small to obtain sufficient red reaction products that the human eyes can observe. Thus, we suggest that the LOD of SiO_2@MCM-41 is 2 ppm, which exhibits high sensitivity for SO_2 naked-eye detection.

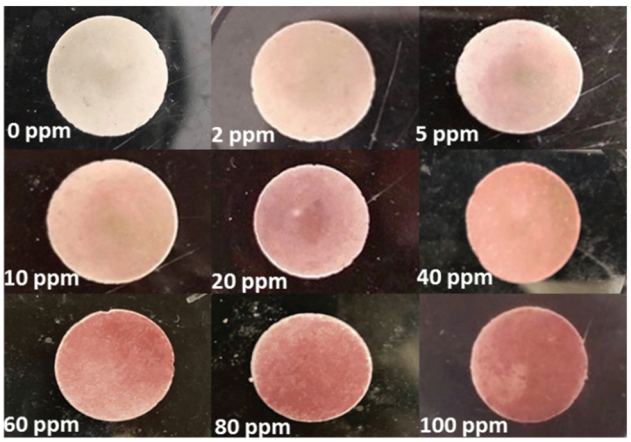

Fig. 4 The visual color changes of SiO_2@MCM-41 discs in response to low concentrations of SO_2 gases.

By observing the color change of the SiO_2@MCM-41 solid, we can estimate the approximate concentration of SO_2 gas. However, for a practical, visual and rapid SO_2 gas sensor, it should be able to detect SO_2 quantitatively. Therefore, we proposed an SO_2 GDT. The apparatus consists of a transparent glass tube with iron meshes at both ends, and the SiO_2@MCM-41 solid samples were fixed between the iron meshes. After the injection of different concentrations of SO_2 gases through a 100 mL syringe, the color of the SO_2 GDT turned to red at different lengths (Fig. 5a). The response lengths of the red portions toward 100, 200, 400, 800 and 1000 ppm are about 1.6, 3.2, 6.5, 12.5 and 17.4 mm, respectively. By measuring the length of the product, we can infer the concentration of SO_2 gas quantitatively. Fig. 5b shows the relationship between the SO_2 concentration and the color change length of the SO_2 GDT. According to the calibration curve, a very good linear correlation with R^2 = 0.9971 is achieved, which reveals a good potential application for *in situ* SO_2 gas monitoring. Besides, the red reaction product of the GDT cannot remain stable in air for a long time. So after exposure to air for 2 days, the red reaction product vanished, and the SO_2 GDT could be reused again.

Conclusions

This paper reports a core–shell SiO_2@MCM-41 sensor synthesized by an easily operated method and loaded with $ZnCl_2$, SNP and hexamine as indicators. The SiO_2@MCM-41 sensor was made into solid powder, discs and a GDT. The as-prepared three SiO_2@MCM-41 sensors were measured by exposure to different concentrations of SO_2 gas, and the sensing properties

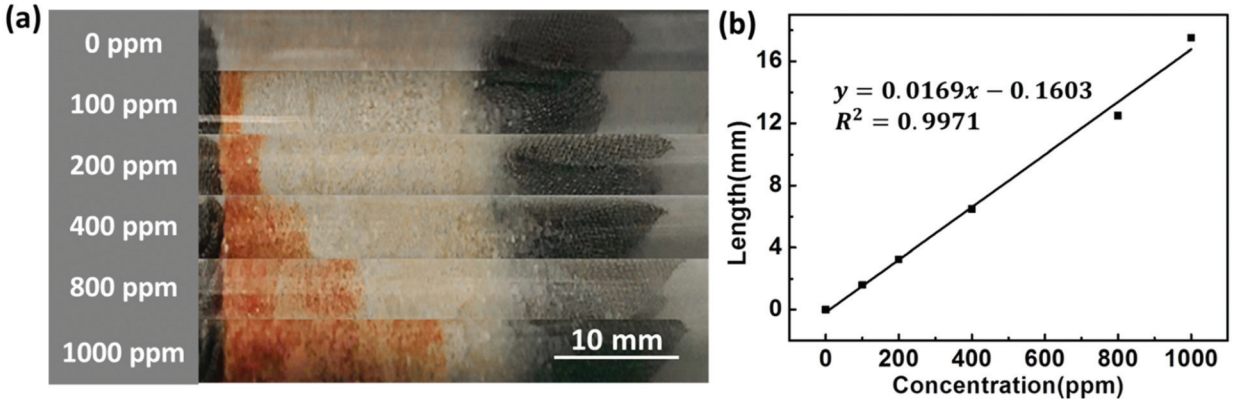

Fig. 5 (a) The visual color change length and (b) corresponding fitting curve of the SO_2 GDT in response to various concentrations of SO_2 gases.

were systematically investigated. As a result, the SiO_2@MCM-41 sensor displayed different color changes with various concentrations and a quick response. The LOD of SiO_2@MCM-41 is 2 ppm, which indicated that the sensor is highly sensitive. Moreover, the SO_2 GDT performed colorimetric quantitative detection, and hence we suggest the potential application of practical SO_2 sensing. In summary, this SiO_2@MCM-41 sensor is easy to fabricate and operate. The research results in this paper show high sensitivity, outstanding stability and perfect response concentration linearity to SO_2. Besides, the distinct color change of SiO_2@MCM-41 after exposure to SO_2 makes naked-eye detection possible. Thus, we believe it is a qualified candidate for SO_2 *in situ* monitoring.

Conflicts of interest

There are no conflicts to declare.

Acknowledgements

The financial support was obtained from the National Natural Science Foundation of China (U1530141, 21874009 and 21804009).

References

1 D. Zhang, J. Wu, P. Li and Y. Cao, *J. Mater. Chem. A*, 2017, **5**, 20666–20677.
2 K. G. Anne, S. Krenn and H. Puxbaum, *Fresenius' J. Anal. Chem.*, 1999, **363**, 73–76.
3 M. R. Tchalala, P. M. Bhatt, K. N. Chappanda, S. R. Tavares, K. Adil, Y. Belmabkhout, A. Shkurenko, A. Cadiau, N. Heymans, G. D. Weireld, G. Maurin, K. N. Salama and M. Eddaoudi, *Nat. Commun.*, 2019, **10**, 1328–1337.
4 A. V. Leontiev and D. M. Rudkevich, *J. Am. Chem. Soc.*, 2015, **127**, 14126–14127.
5 J. Nisar, Z. Topalian, A. De Sarkar, L. Osterlund and R. Ahuja, *ACS Appl. Mater. Interfaces*, 2013, **5**, 8516–8522.
6 J. N. Yun, C. Zhu, Q. Wang, Q. L. Hu and G. Yang, *Catal. Commun.*, 2018, **114**, 79–83.
7 C. Ma, X. D. Hao, X. Yang, X. H. Liang, F. M. Liu, T. Liu, C. H. Yang, H. Q. Zhu and G. Y. Lu, *Phys. Chem. Chem. Phys.*, 2014, **16**, 19327–19332.
8 L. Ping, X. Fei, P. Jiayong, C. Yiping, P. Huaming and C. Shaohua, *Environ. Sci. Manage.*, 2011, **36**, 30–35.
9 Y. Uneme, S. Tamura and N. Imanaka, *Sens. Actuators, B*, 2013, **177**, 529–534.
10 J. Zhang, Z. Qin, D. Zeng and C. Xie, *Phys. Chem. Chem. Phys.*, 2017, **19**, 6313–6329.
11 J. L. Martínez-Hurtado, C. Davidson, J. Blyth and C. R. Lowe, *Langmuir*, 2010, **26**, 15694–15699.
12 T. Dinh, I. Choi, Y. Son and J. Kim, *Sens. Actuators, B*, 2016, **213**, 529–538.
13 U. Tumuluri, J. D. Howe, W. P. Mounfield III, M. J. Li and A. C. S. Sustain, *Chem. Eng.*, 2017, **5**, 9295–9306.
14 T. Wang, D. Huang, Z. Yang, S. Xu, G. He, X. Li, N. Hu, G. Yin, D. He and L. Zhang, *Nano-Micro Lett.*, 2016, **8**, 95–119.
15 C. T. Kresge, M. E. Leonowicz, W. J. Roth, J. C. Vartuli and J. S. Beck, *Nature*, 1992, **359**, 710–712.
16 L. Li, M. Krissanasaeranee, S. W. Pattinson, M. Stefik, U. Wiesner, U. Steiner and E. Dominik, *Chem. Commun.*, 2010, **46**, 7620–7622.
17 Y. K. Lu and X. P. Yan, *Anal. Chem.*, 2004, **76**, 453–457.
18 Y. Li, W. Luo, N. Qin, J. Dong, J. Wei, W. Li, S. Feng, J. Chen, J. Xu, A. A. Elzatahry, M. H. Es-Saheb, Y. Deng and D. Zhao, *Angew. Chem., Int. Ed.*, 2014, **53**, 9035–9040.
19 S. Shao, M. Dimitrov, N. Guan and R. Köhn, *J. Mater. Chem.*, 2009, **19**, 8411–8410.
20 Z. Hou, C. Li, P. Ma, Y. Dai, D. Yang, Z. Cheng and J. Lin, *Adv. Funct. Mater.*, 2012, **22**, 2713–2722.
21 J. Zhao, T. Yang, Y. Liu, Z. Wang, X. Li, Y. Sun, Y. Du, Y. Li and G. Lu, *Sens. Actuators, B*, 2014, **191**, 806–812.
22 N. Izu, G. Hagen, D. Schönauer, U. Röder-Roith and R. Moos, *Sensors*, 2011, **11**, 2982–2991.
23 R. Chaudhuri and S. Paria, *Chem. Rev.*, 2012, **112**, 2373–2433.
24 W. Schartl, *Nanoscale*, 2010, **2**, 829–843.
25 Y. Deng, D. Qi, C. Deng, X. Zhang and D. Zhao, *J. Am. Chem. Soc.*, 2008, **130**, 28–29.
26 J. D. Qiu, H. P. Peng, R. P. Liang and X. H. Xia, *Biosens. Bioelectron.*, 2010, **25**, 1447–1453.
27 Y. Chen, B. Zhu, M. Yao, S. Wang and S. Zhang, *Catal. Commun.*, 2010, **11**, 1003–1007.
28 Z. Wu, K. Yu, S. Zhang and Y. Xie, *J. Phys. Chem. C*, 2008, **112**, 11307–11313.
29 S. Q. Li, Y. J. Diao, Z. J. Yang, J. M. He, J. Wang, C. C. Liu, F. M. Liu, H. Y. Lu, X. Yan, P. Sun and G. Y. Lu, *Sens. Actuators, B*, 2018, **276**, 526–533.
30 W. StoBer, A. Fink and E. Bohn, *J. Colloid Interface Sci.*, 1968, **26**, 62–69.
31 J. Huang, M. Antonietti and J. Liu, *J. Mater. Chem. A*, 2014, **2**, 7686.
32 Compiling group, *Huaxue Qiye Kongqizhong Youhai Wuzhi Ceding Fangfa*, Chemical Industry Press, Beijing, 1983.
33 Y. Zhao, C. Ge and Y. Liang, *Huaxue Fenxi Jiliang*, 2016, **25**, 77–79.
34 W. Moser, R. A. Chalmers and A. G. Fogg, *J. Inorg. Nucl. Chem.*, 1965, **27**, 1–40.
35 A. G. Fogg, W. Moser and R. A. Chalmers, *Anal. Chim. Acta*, 1966, **36**, 248–251.
36 R. W. Stevens, R. V. Siriwardane and J. Logan, *Energy Fuels*, 2008, **22**, 3070–3079.
37 S. Sjostrom and H. Krutka, *Fuel*, 2010, **89**, 1298–1306.
38 H. G. Stenger, K. Hu and D. R. Simpson, *Gas Sep. Purif.*, 1993, **7**, 19–25.